Green synthesis of stable Fe,Cu oxide nanocomposites from loquat leaf extracts for removal of Norfloxacin and Ciprofloxacin

Qiujie Liu, Peili Ma, Penglei Liu, Hongping Li, Xiuli Han, Lie Liu and Weihua Zou

ABSTRACT

Mass production of nanomaterials to remove pollutants from water still faces many challenges, mainly due to the complexity of the synthesis methods involved and the use of dangerous reagents. The green method of preparation of nanomaterials from plants can effectively solve these problems. Fe,Cu oxide nanocomposites (Fe-Cu-NCs) were synthesized by a green and single-step method using loquat leaf extracts, and were used as an adsorbent for removal of Norfloxacin (NOR) and Ciprofloxacin (CIP) from aqueous solution. The synthesized adsorbent showed excellent adsorption properties for NOR and CIP. The experimental equilibrium data fitted the Redlich-Peterson and Koble-Corrigan models well and the maximum adsorption capacities of Fe-Cu-NCs calculated by the Langmuir model for NOR and CIP were 1.182 mmol/g and 1.103 mmol/g, respectively, at 293 K. Additionally, the morphologies and properties of Fe-Cu-NCs were characterized by transmission electron microscopy (TEM), scanning electron microscopy X-ray energy-dispersive spectroscopy (SEM-EDS), X-ray photoelectron spectroscopy (XPS), X-ray diffraction (XRD) and Fourier transform infrared spectroscopy (FTIR) analysis and the adsorption mechanism of NOR and CIP onto Fe-Cu-NCs was discussed. Thermodynamic parameters revealed that the adsorption process was spontaneous and endothermic. This study indicated that Fe-Cu-NCs are a potential adsorbent and provide a simple and convenient strategy for the purification of antibiotics-laden wastewater.

Key words | adsorption mechanism, Ciprofloxacin, Fe,Cu oxide nanocomposites, loquat leaf, Norfloxacin

Qiujie Liu
Peili Ma
Penglei Liu
Hongping Li
Xiuli Han
Lie Liu
Weihua Zou (corresponding author)
School of Chemical Engineering,
Zhengzhou University,
100# of Kexue Road, Zhengzhou, 450001,
China
E-mail: *whzou@zzu.edu.cn*

INTRODUCTION

Antibiotics are widely used in medicine, animal husbandry and aquaculture to prevent and treat bacterial infectious diseases (Zheng *et al.* 2013). But in recent years, antibiotics have been abused all over the world and released to surface water through different routes, such as hospital and industrial antibiotic waste, human and animal metabolic waste, agricultural activities (Anthony *et al.* 2018). Water containing trace amounts of antibiotics can indirectly affect human health by causing a decline of the body's immune system (Kong *et al.* 2016). Quinolones, the most widely used antibiotics class, have been classified among the most important synthetic antibiotics used in human and veterinary medicine (Homem & Santos 2011). Norfloxacin (NOR) and Ciprofloxacin (CIP) are synthetic, broad-spectrum antibacterial agents of the fluoroquinolones family. Factors including the sewage discharge of drug manufacturers, effluents from hospitals and incomplete metabolism in animals are major causes of the omnipresence of NOR and CIP residues in aquatic ecosystems (Wan *et al.* 2018). Therefore, it is necessary to explore effective techniques for antibiotic removal from wastewaters.

Adsorption is considered to be one of the effective methods for the treatment of contaminants, due to its features of low cost, easy operation, strong practicability and high efficiency (Wan *et al.* 2018). Over the past decade, numerous attempts have been made to develop low-cost and effective adsorbents, including nanomaterials or nanocomposites for the removal of contaminants from water. Compared with the traditional materials, nanostructured adsorbents exhibit much higher efficiency and faster removal rate in water treatment (Zhang *et al.* 2016).

doi: 10.2166/wst.2020.152

So far, nanomaterials, including carbon nanomaterials (Jha *et al.* 2019), magnetic nanomaterials (Gutiérrez *et al.* 2018), polydopamine microspheres (Wan *et al.* 2018), metal oxide nanomaterials (Khandare & Mukherjee 2019) have been studied. Among these nanomaterials, metal oxide nanomaterials are the most commonly used and can be readily synthesized by various chemical and physical methods. However, the physical and chemical methods are generally expensive and have a high energy consumption. Moreover, the reducing agents used in the preparation process are mostly toxic and corrosive chemicals, and the nanomaterials obtained have a definite impact on the environment (Wang *et al.* 2014). Hence, it is imperative to develop a green and efficient preparation method for nanoadsorption.

Green nanotechnology involves the development of novel and environmentally friendly methods for the preparation of nanomaterials (Singh *et al.* 2017). Thus, the green synthesis of metal nanoparticles, including microbial and plant synthesis, is considered to be a greener, safer and more cost-effective method to replace chemical and physical production methods. Particularly, plant extracts are promising for the synthesis of nanoparticles since they are cheap, simple to use and scalable.

Considerable efforts have been made to develop plant synthesis methods for the rapid and large-scale fabrication of nanomaterials without the use of dangerous reagents. It has been found that plant extracts that contain the most abundant chemical constituents, such as reducing sugars, phenols, flavonoids and proteins, could serve as the reducing and capping agents for the synthesis of nanoparticles (Makarov *et al.* 2014). For instance, CuO nanoparticles for the effective removal of As(III) were synthesized from *Tamarindus indica* pulp extracts (Singh *et al.* 2017); iron nanoparticles for the removal of hexavalent chromium were synthesized using *Eichhornia crassipes* extracts (He *et al.* 2018); Fe,Cu-based nanoparticles for the removal of malachite green were synthesized using *Parthenocissus quinquefolia* leaf extracts (Zhang *et al.* 2018). These researchers demonstrated that green synthesis is feasible, and provides a basis for the synthesis of metal oxide nanoparticles from plant extracts for contaminant removal (Luo *et al.* 2015).

Loquat (*Eriobotrya japonica*) is a large evergreen shrub that contains a high amount of polyphenols or related antioxidants; these could serve as both reducing and capping agents (Awwad *et al.* 2013), so loquat leaf is a good material for the preparation of metal oxide nanoparticles. CuO and Fe_2O_3 are very stable oxides in normal environmental conditions (Singh *et al.* 2017), and Fe_2O_3 has a high reaction surface area and high removal rate, favorable properties and non-toxicity (Nalbandian *et al.* 2016). Thus in the current study, Fe,Cu oxide nanocomposites (Fe-Cu-NCs) were chosen as an adsorbent for the adsorption of NOR and CIP from aqueous solution. To our knowledge, the preparation of Fe,Cu oxide nanocomposites using loquat leaf extracts has not previously been reported in the literature.

In this study, Fe-Cu-NCs were synthesized from loquat leaf extracts and used as the adsorbent for the removal of NOR and CIP. The adsorption kinetics, isotherms and thermodynamic properties of Fe-Cu-NCs for NOR and CIP removal were explored. Furthermore, the adsorption mechanism is discussed according to the results of adsorption experiment.

MATERIALS AND METHODS

Materials and reagents

Ferric chloride hexahydrate ($FeCl_3{\cdot}6H_2O$) and cupric chloride dihydrate ($CuCl_2{\cdot}2H_2O$) were purchased from Shanghai Macklin BioChem Technology Co. Ltd (Shanghai, China); Norfloxacin ($C_{16}H_{18}FN_3O_3$, 319.33 g/mol, ≥98%) and Ciprofloxacin ($C_{16}H_{18}FN_3O_3$, 367.82 g/mol, ≥98%) were obtained from Haizhengshenghua Biotechnology Limited (Henan Province, China). Oxalic acid (ethanedioic acid) was purchased from Tianjin Kermel Chemical Reagent Company (Tianjin, China). All chemicals used in this study were analytical grade.

PREPARATION METHODS

Preparation of loquat leaf extracts

Fresh loquat leaves were washed with distilled water and dried to constant weight at 323 K. Then 70 g dried loquat leaves were added to 1 L of deionized water and heated for 150 min at 333 K under sealed conditions. The extracts were filtered and stored in the refrigerator for further use.

Synthesis of adsorbents

Oxalic acid (0.02 mol) was added to 150 mL of the extracts of loquat leaf under vigorous stirring at ambient temperature. After 30 min, 70 mL of $FeCl_3$ and $CuCl_2$ premixed solution (0.095 mol/L) was added dropwise to the extracts over a 3 hour period under continued vigorous stirring. The color of the solution changed from clear to atrovirens (dark brown)

and the reaction mixture was stirred for another 1 hour. The precipitated mass was then separated by centrifugation (10,000 rpm for 4 min) and washed with deionized water three times. Finally, the product was freeze-dried and stored.

Synthesis mechanism of Fe-Cu-NCs

Loquat leaf extracts contain a potent array of polyphenolic compounds that may act as reducing agent: first the hydroxyl groups of the polyphenolic compounds formed the complex with the Cu^{2+} and Fe^{3+} and then reduced them to Cu and Fe. These metallic copper and iron atoms reacted with the available oxygen in the atmosphere to form the most stable oxides i.e. CuO and Fe_2O_3 (Singh *et al.* 2017). The preparation mechanism diagram is shown in Figure 1.

Characterization analysis

Scanning electron microscope (SEM) (Zeiss Merlin Compact) equipped with an X-ray energy-dispersive spectrometer (EDS) (Bruker Nano GmbH Berlin, Germany) and a transmission electron microscope (TEM) (FEI Tecnai G2 F20) were employed to analyse the surface structure and morphology of samples. The structural composition of Fe-Cu-NCs were measured by X-ray diffraction (XRD) (Bruker D8 Advance). X-ray photoelectron spectroscopy (XPS) (Thermo Escalab 250 XI) was employed to determine the surface chemical elemental composition. Fourier transform infrared spectroscopy (FTIR) (PE-1710 spectrophotometer, USA) was employed to identify the surface functional groups of Fe-Cu-NCs. The specific surface area and pore size distributions of Fe-Cu-NCs was determined by nitrogen adsorption–desorption isotherms at 77 K using a surface area analyzer (NOVA1200e, USA). The point of zero charge (pH_{PZC}) of Fe-Cu-NCs was determined using the salt addition method; the value obtained pH_{PZC} was 3.74.

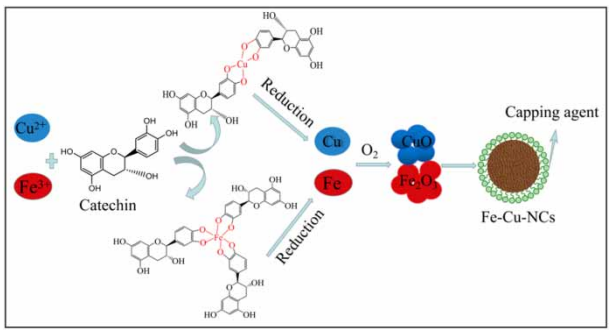

Figure 1 | Schematic illustration of plausible synthesis mechanism.

Adsorption experiments

Batch adsorption experiments were carried out in a 50 mL Erlenmeyer flask, containing 5 mg of Fe-Cu-NCs and 20 mL diluted NOR or CIP solutions, that was subjected to shaking in a mechanical constant temperature vibrator. After 180 min adsorption equilibrium, the mixture was centrifuged at 10,000 rpm for 3 min. The effect of initial pH on the removal of NOR or CIP was analyzed in the pH range of 2–12. The adsorption kinetic experiments were conducted with initial concentrations of NOR and CIP of 0.313, 0.470 and 0.626 mol/L at 293 K, respectively. Samples were taken periodically, until an adsorption equilibrium was reached. Equilibrium isotherm experiments were performed with different initial concentrations of NOR or CIP solution (ranging from 0.063 to 0.783 mmol/L) for 180 min at 293, 303 and 313 K. The effect of ionic strength was studied with different salt concentrations (varying from 0 to 0.1 mol/L) of NaCl and $CaCl_2$. All the experiments were carried out under identical conditions and repeated three times. The remaining concentration of NOR and CIP were measured by ultraviolet-visible spectrophotometer (TU-1810, Puxi General Instrument Co. Ltd, Beijing, China) both using wavelengths of 276 nm.

Data analysis

The adsorption capacity q_t (mmol/g) and the removal efficiency η of NOR or CIP were determined by the following equations:

$$q_t = \frac{(C_0 - C_t)V}{m} \quad (1)$$

$$\eta = \frac{100(C_0 - C_t)}{C_0}\% \quad (2)$$

where q_t (mmol/g) is the adsorption capacity. C_0 (mmol/L) and C_t (mmol/L) are the NOR or CIP concentrations in the solution at the start and any time t, respectively. V (L) is the volume of the NOR or CIP solution, and m (g) is the mass of the adsorbent. η is the removal efficiency.

The degree of fit of the kinetic and isotherm models was evaluated by relative standard deviation ARS, which is

defined as follows:

$$ARS = \sqrt{\frac{\sum_{1}^{n}[(q_{exp} - q_{cal})/q_{exp})^2]}{n-1}} \quad (3)$$

where n is the number of data points, and q_{exp} and q_{cal} (mmol/g) are the experimental and calculated adsorption capacities, respectively.

RESULTS AND DISCUSSION

Characterization of adsorbents

Morphology analysis

The surface morphology of Fe-Cu-NCs samples was characterized by SEM (Figure 2), which revealed the successful synthesis of Fe-Cu-NCs. It is clearly evident that the nanocomposites appear spheroidal, with a diameter ranging from 100 to 200 nm, and they tend to form a homogeneous size distribution. TEM images (Figure 2(c)) showed that the Fe-Cu-NCs were polydispersed particles and the surface of Fe-Cu-NCs was capped with organic matter. The organic matter capping on the surface of nanocomposites played a crucial role in preventing their aggregation, improving their dispersion and stability (Weng *et al.* 2017; Zhang *et al.* 2018).

To further understand the element composition of Fe-Cu-NCs, the localized elemental information of Fe-Cu-NCs was determined by EDS, as shown in Figure 2(d). There are intense peaks of C, O, Fe and Cu, confirming the presence of Fe and Cu. The signals of elemental C and O originated from the polyphenol groups and other C-, O-containing molecules in loquat leaf extracts (Weng *et al.* 2017). The weight composition of C and O is more than that of Fe and Cu, which may be attributed to the fact that the surface of Fe-Cu-NCs was coated with biomolecules of loquat leaf extracts (Weng *et al.* 2017).

XPS and XRD analysis

Figure 3 shows the XPS patterns of Fe-Cu-NCs. In Figure 3(a), due to the low content of copper, the characteristic peak of Cu 2p was not shown in the spectra. Figure 3(b) shows the spectra of Fe and Cu of Fe-Cu-NCs: the core levels

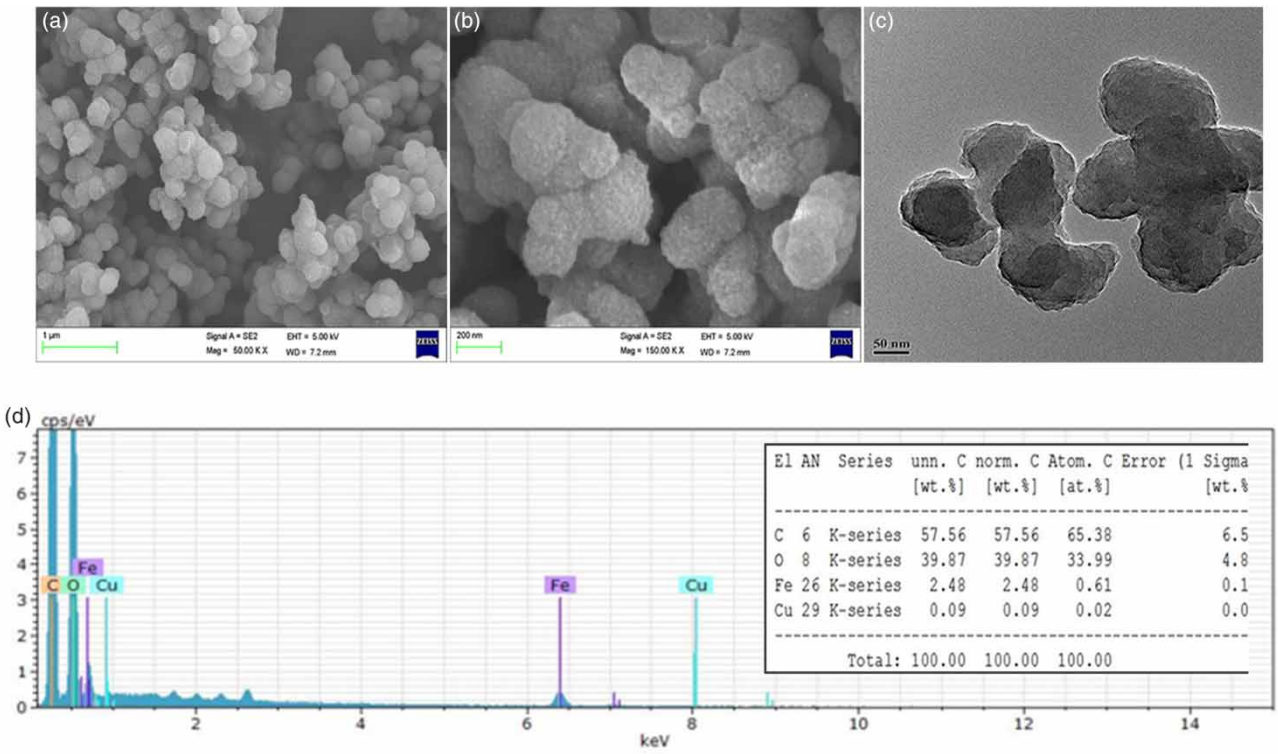

Figure 2 | (a), (b) SEM images of Fe-Cu-NCs; (c) TEM images of Fe-Cu-NCs; (d) EDS analysis of Fe-Cu-NCs.

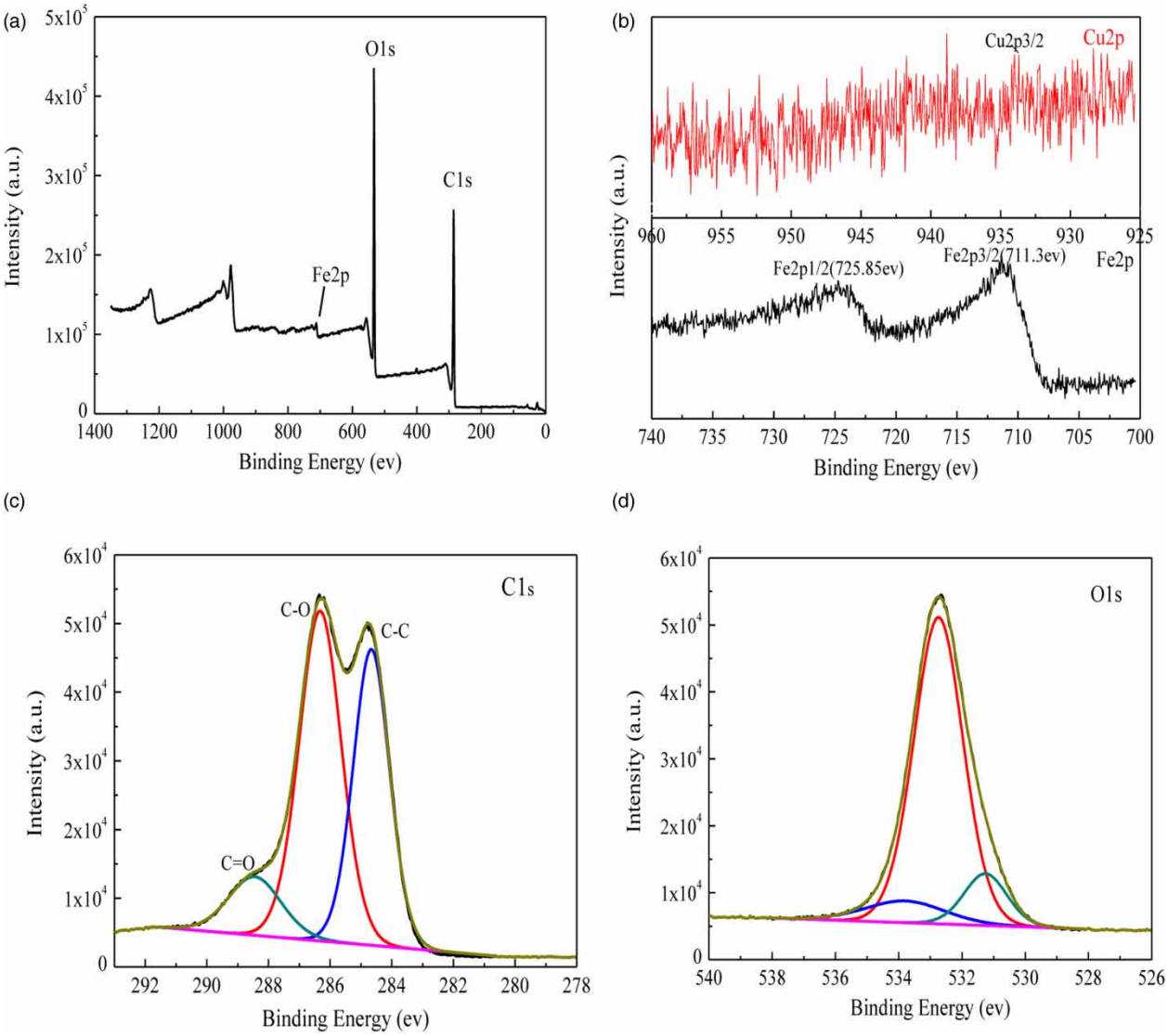

Figure 3 | XPS spectra of the Fe-Cu-NCs: (a) widescan; (b) Fe 2p and Cu 2p spectrum; (c) C 1s spectrum; (d) O 1s spectra.

of Fe 2p3/2 and Fe 2p1/2 were 711.3 eV and 725.85 eV, respectively, corresponding to Fe^{3+}, and consistent with the peaks reported for iron oxide (Fang *et al.* 2011; Luo *et al.* 2015). As shown in Figure 3(c), there were three C peaks on the C 1s curves, corresponding to C-C, C-O and C = O, respectively, implying that biomolecules were attached to the surface of Fe-Cu-NCs (Awwad *et al.* 2013). Additionally, the O 1s XPS spectrum was further analysed in Figure 3(d), where components were attributed respectively to OH^- (531.25 eV) and C-O (532.75 eV) (Grosvenor *et al.* 2004). The presence of O 1s and C 1s implied that some biomolecules and oxalates formed a strong coating on the surface of Fe-Cu-NCs by chemical bonding (Khandare & Mukherjee 2019).

XRD data were collected in the 2θ range of 5–90°, and the pattern is shown in Figure 4. It can be seen that the whole pattern is deficient in distinctive diffraction peaks, suggesting that the synthesized Fe-Cu-NCs are mainly amorphous in nature, as previously reported for the eucalyptus extract synthesized nanoparticles (Wang *et al.* 2014). A broad shoulder peak at around $2\theta = 25°$ can be ascribed to organic molecules adsorbed from the loquat leaf extracts as a capping or stabilizing agent (Wang *et al.* 2014).

FTIR analysis

The FTIR spectra of Fe-Cu-NCs is shown in Figure 5. A obvious peak at 3,332 cm^{-1} is attributed to O-H stretching

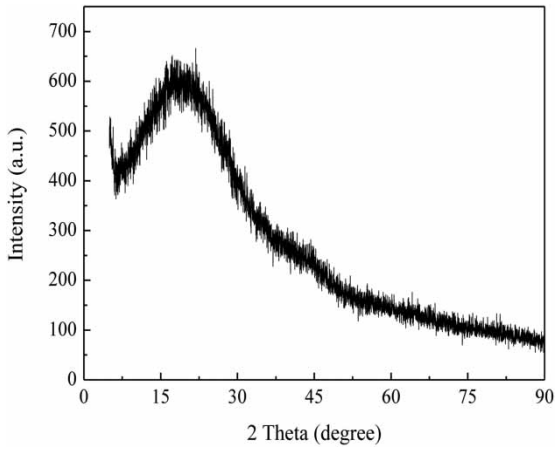

Figure 4 | XRD analysis of the Fe-Cu-NCs.

vibration (Mohan Kumar *et al.* 2013). One prominent peak at 1,627 cm^{-1} indicates the O-H and C = C stretching vibration of an aromatic ring, which is thought to be related to polyphenols or sugars/glycosides originating from the loquat leaf extracts (Awwad *et al.* 2013). The peaks at 1,275 cm^{-1} and 820 cm^{-1} are ascribed to C = O of the carboxylic acid and C-C stretching modes, respectively (Zhang *et al.* 2018), then the band at 1,075 cm^{-1} is mainly produced by O-H bending vibration and C-O-C stretching vibration. Finally an absorption band around 613 cm^{-1} corresponds to Fe-O stretches of iron oxides (Yadav *et al.* 2015).

Figure 5 also shows FTIR spectra of Fe-Cu-NCs adsorption of NOR or CIP. In comparison with FTIR spectra of Fe-Cu-NCs, the band at 1,627 cm^{-1} has shifted to a lower wavelength, revealing an interaction between −OH groups and the CIP or NOR molecules, thus it can be reasonably inferred that the CIP or NOR adsorption process occurs via electrostatic interactions (Zhang *et al.* 2018). In addition, several new bands appeared, corresponding to NOR or CIP. For

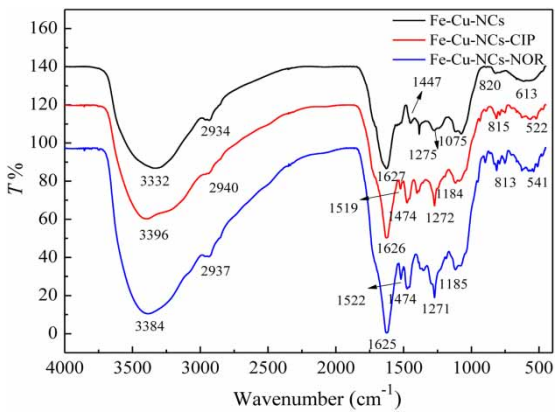

Figure 5 | FTIR spectra of Fe-Cu-NCs and Fe-Cu-NCs after adsorption of NOR and CIP.

the Fe-Cu-NCs adsorbed with NOR, the new peak at 1,185 cm^{-1} belonging to the C-F bonds proved the presence of NOR on the adsorbents. FTIR analysis not only strongly confirmed that the molecular structure of Fe-Cu-NCs contains C = C, C-H, Fe-O and oxygen containing functional groups, but also confirmed the adsorption of NOR or CIP onto Fe-Cu-NCs.

BET analysis

Nitrogen adsorption-desorption isotherm with BET analysis was used to determine the specific surface area of Fe-Cu-NCs. As can be seen in Figure 6, the curve was characteristic of type-IV isotherm accompanying a H4 type hysteresis loop (Zhang *et al.* 2018), which was ascribed to capillary condensation, indicating the existence of a mesoporous matrix in the samples (Sai Saraswathi *et al.* 2017). The BET surface area of the Fe-Cu-NCs was 13.38 m^2/g and the pore volume was 0.055 cm^3/g. The as-prepared mesoporous structure had a narrow pore size distribution range and the average pore diameter was 1.54 nm. In addition, the desorption curve of the isotherm has a prominent point, indicating that the pore size of the material was heterogeneous and disordered.

ADSORPTION EXPERIMENTS

The effect of pH value and adsorption mechanism

Solution pH is a critical factor during the adsorption process, because the change of pH of the aqueous solution influences the speciation of NOR or CIP and the surface

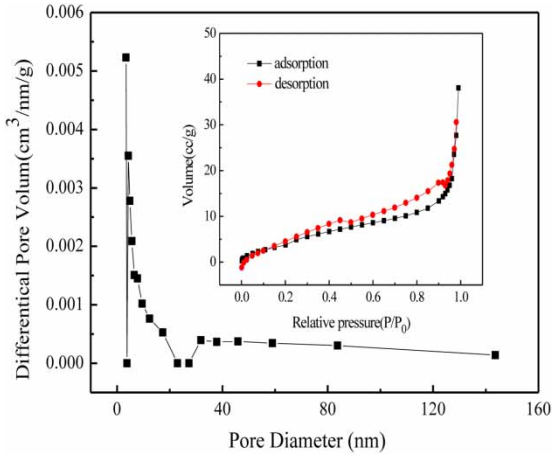

Figure 6 | Nitrogen adsorption and desorption isotherms and pore volume distributions of Fe-Cu-NCs.

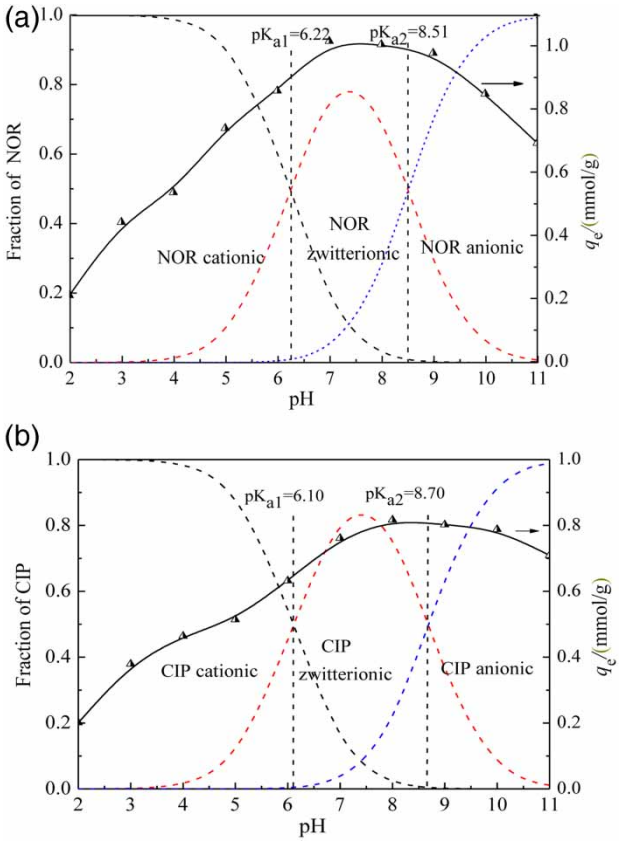

Figure 7 | (a) The effect of pH on the NOR adsorption and the distribution coefficient of NOR; (b) the effect of pH on the CIP adsorption and the distribution coefficient of CIP.

charge of Fe-Cu-NCs (Yuan *et al.* 2019). NOR and CIP are amphoteric molecules and there are two proton-binding sites (carboxyl and piperazinyl groups) that can be present as cations, zwitterions and anions at different pH values (Meng *et al.* 2018). As shown in Figure 7, the adsorption capacity of NOR onto Fe-Cu-NCs was increased from 0.21 mmol/g to 1.015 mmol/g when the pH values were raised from 2 to 7. Conversely, as the pH increased from 7 to 11, the adsorption capacity of NOR onto Fe-Cu-NCs was decreased from 1.015 mmol/g to 0.692 mmol/g and the adsorption efficiency was decreased by 31.8%. It can be seen that the optimal pH value for the adsorption of NOR onto Fe-Cu-NCs was 7, and the adsorption capacity did not decrease significantly when the pH values were raised from 7 to 11. This result indicates that the adsorption of NOR onto Fe-Cu-NCs is suitable for neutral or weakly alkaline conditions.

Similarly, the adsorption capacity of CIP onto Fe-Cu-NCs was increased from 0.201 mmol/g to 0.817 mmol/g when the pH values were raised from 2 to 8. By contrast, when the pH values were increased from 8 to 11, the adsorption capacity of CIP onto Fe-Cu-NCs was decreased from 0.817 mmol/g to 0.709 mmol/g, and then the adsorption efficiency was only reduced by 13.2%. Thus the optimal pH value for the adsorption of CIP onto Fe-Cu-NCs was 8.

As shown in Figure 7, taking NOR as an example, when $pH < pK_{a1}$, the cation (NOR^+) is the dominant species in the aqueous solution due to the protonation of the piperazinyl nitrogen. When $pK_{a1} < pH < pK_{a2}$, NOR existed mainly as a zwitterion ($NOR^{\pm}$) due to the deprotonation of the carboxylic group and the protonation of the peripheral piperazine. When $pH > pK_{a2}$, the anion (NOR^-) state is due to the increasing deprotonation of carboxylic groups in solution.

The pH_{PZC} is an important parameter of adsorbents, as it characterizes the acidic and basic properties of adsorbents beyond a definite pH value. The pH_{PZC} value was determined to be 3.74. When $pH < pH_{PZC}$, the NOR cation was the dominant species in solution and the surface of the Fe-Cu-NCs also contained positive charges. Therefore the electrostatic repulsion between the adsorbent and adsorbate reduced the adsorption capacity. At $pK_{a1} < pH < pK_{a2}$, the removal efficiency of NOR was increased by its zwitterionic form, and NOR in zwitterionic form was more hydrophobic than its cation or anion form (Yang *et al.* 2012). In addition, NOR could form hydrogen bonds with the hydroxyl groups on the surface of Fe-Cu-NCs via its piperazinyl group, carboxyl group and fluorine group (Liu *et al.* 2019). Moreover, the hydroxyl groups of Fe-Cu-NCs could act as n-electron-donors and the delocalized π bond of the aromatic ring of NOR could serve as an π-electron acceptor due to the strong electron-withdrawing capability of the fluorine group on benzene ring (Yang *et al.* 2012). At $pH > pK_{a2}$, the NOR existed as anionic form, so it and the negative charge on the Fe-Cu-NCs surface repelled each other, resulting in a decrease in adsorption capacity.

In addition to the electrostatic effect, metal surface complexation is responsible for another main mechanism of NOR adsorption in aqueous solutions. NOR is likely to form an energetically favorable mononuclear bidentate complex (i.e., a six-membered ring) with the Fe atom and the Cu atom (Liu *et al.* 2011). The adsorption mechanism of CIP onto Fe-Cu-NCs is similar to that of NOR, and both their adsorption mechanisms are shown in Figure 8.

Adsorption kinetics study

The experimental kinetic data for NOR or CIP adsorption onto Fe-Cu-NCs are shown in Figure 9. It can be seen that

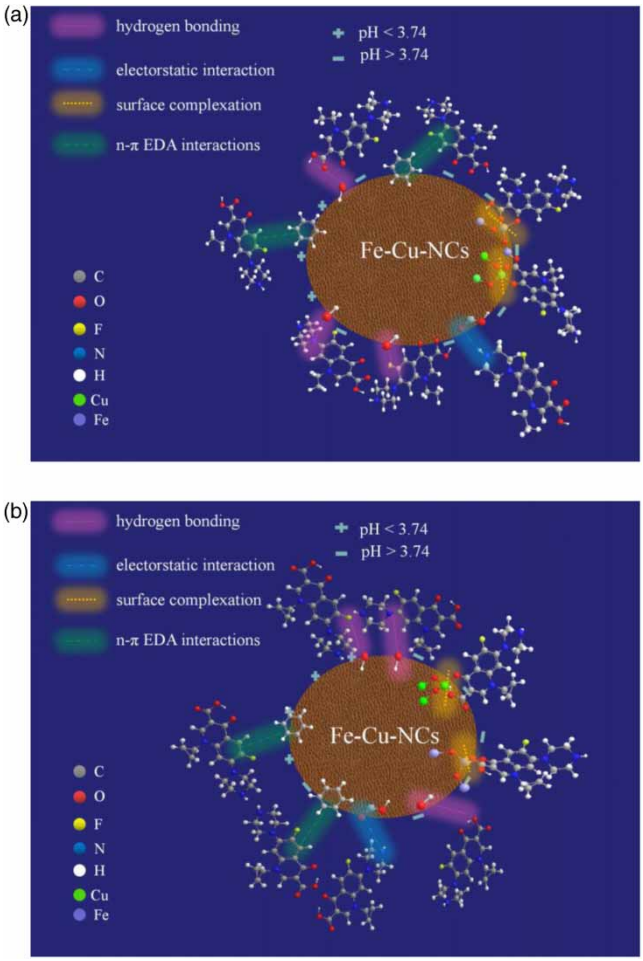

Figure 8 | Schematic illustration of the adsorption mechanism of (a) NOR and (b) CIP onto Fe-Cu-NCs.

the rate of NOR adsorption onto the Fe-Cu-NCs was rapid during the first 10 min, and the adsorption capacity of NOR reached 57.9% of the equilibrated adsorption when the initial concentration was 0.470 mmol/L at 293 K. Under the same conditions, the CIP uptake reached 64.8% of the equilibrated adsorption amounts during the first 10 min. The experimental results support the fact that the initial stage of adsorption is a rapid process. However, due to the decrease in the number of the adsorption sites, the increasing trend slowed down until a state of equilibrium was reached after 180 min for both NOR and CIP (Al-Musawi *et al.* 2017). It can be seen that NOR or CIP adsorption amounts at equilibrium (q_e) were increased from 0.906 to 1.153 mmol/g and from 0.592 to 0.871 mmol/g with an increase in the initial NOR or CIP concentrations from 0.313 to 0.626 mmol/L, respectively, suggesting that the greater concentration gradient could overcome mass transfer resistances during the adsorption process (Sepehr *et al.* 2014). Compared with the kinetic experimental data of NOR and CIP at the same concentration, the adsorption capacity of NOR is higher than that of CIP, which may be attributed to the lower molecular weight of NOR relative to CIP.

In order to investigate the mechanism of the adsorption process of NOR and CIP onto the Fe-Cu-NCs, the experimental kinetic data were fitted according to the pseudo-first-order model, pseudo-second-order model, double-constant rate equation, Elovich model, and the intra-particle diffusion model. These model are described by the following equations:

$$\text{Pseudo-first-order model: } q_t = q_e(1 - e^{-k_1 t}) \tag{4}$$

$$\text{Pseudo-second-order model: } q_t = \frac{k_2 q_e^2 t}{1 + k_2 q_e^2 t} \tag{5}$$

$$\text{Double-constant rate equation: } q_t = \alpha t^{k_s} \tag{6}$$

$$\text{Elovich model: } q_t = \frac{\ln(A + B)}{B} + \frac{\ln(t)}{B} \tag{7}$$

$$\text{Intra-particle diffusion model: } q_t = k_t t^{1/2} + C \tag{8}$$

where q_t and q_e (mmol/g) are the adsorption capacities at time t (min) and at equilibrium, respectively. The k_1 (min^{-1}) and k_2 (g/(mmol/min)) are the rate constants of pseudo-first-order model and pseudo-second-order model, respectively. A (mmol/(g/min)) is the initial adsorption rate of the Elovich model and B (g/min) is the extent of surface coverage. The α and k_s are the correlation constants of the double-constant rate equation. k_t (mg/(g $\text{min}^{1/2}$)) is the intra-particle diffusion rate constant and C is related to the boundary layer thickness.

The corresponding parameters obtained from fitted models are shown in Table 1. A higher value of R^2 and a smaller value of ARS indicated the higher accuracy of kinetic models: it can be seen that the adsorption process of Fe-Cu-NCs for NOR and CIP were fitted best to the double-constant rate equation and Elovich model. The Elovich model describes a series of adsorption processes on heterogeneous adsorbing surfaces, such as bulk or interfacial diffusion and surface activation and deactivation (Sun *et al.* 2019), so it indicated that the adsorption process of NOR or CIP onto Fe-Cu-NCs was heterogeneous. The double-constant rate equation is derived from the Freundlich equation. The kinetic rate constant k_s reflects the adsorption rate, and the higher the k_s value is, the faster

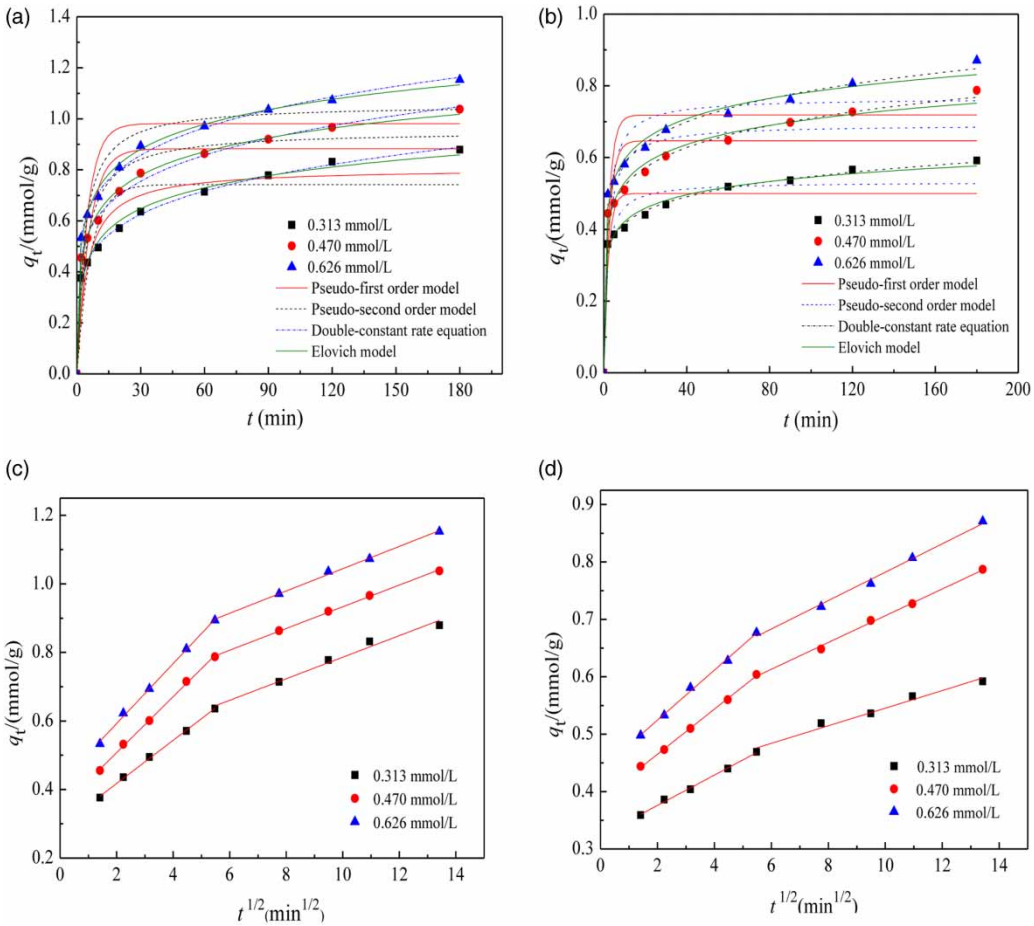

Figure 9 | (a) Adsorption kinetic curves for the adsorption of NOR onto Fe-Cu-NCs; (b) adsorption kinetic curves for the adsorption of CIP onto Fe-Cu-NCs; (c) fitting curves of intra-particle diffusion for NOR adsorption; (d) fitting curves of intra-particle diffusion for CIP adsorption.

the adsorption reaction. The intercept α reflects the adsorption capacity, and the larger the intercept is, the stronger the adsorption capacity (Sun *et al.* 2019).

To better understand the adsorption process, the intra-particle diffusion model was applied to get further insights into the adsorption behavior of NOR and CIP onto Fe-Cu-NCs. As shown in Figure 9(c) and 9(d), the adsorption process can be divided into two adsorption stages for the same initial concentration. The first stage can be attributed to a rapid diffusion of NOR or CIP through the solution to the external surface of Fe-Cu-NCs. The second stage involves the internal diffusion of NOR or CIP molecules into the interior of the adsorbent particles. As can be seen from Table 1, the k_{t1} value of the intra-particle diffusion model was higher than the corresponding k_{t2}, and boundary layer effect constant C_2 was higher than the corresponding C_1. These results indicated that in the first stage, the mass transfer of NOR or CIP molecules from the bulk solution to the Fe-Cu-NCs surface dominated the initial adsorption process, because not only was the intra-particle diffusion rate relatively fast, but also the boundary layer effect seemed weak. At the second stage, steric hindrance exerted by NOR or CIP molecules to the Fe-Cu-NCs surface caused viscous drag to the adsorption process (Wang & Yan 2011). The fitting curves of the intra-particle diffusion were multi-linear and did not pass through the origin, indicating that intra-particle diffusion is not the only rate-limiting step for the process of adsorption (Sepehr *et al.* 2014). Moreover, the parameters k_{t1} and k_{t2} of NOR were greater than that of CIP, implying that the mass transfer resistance of NOR was smaller.

Adsorption isotherm study

The adsorption isotherms of NOR and CIP from the solution onto Fe-Cu-NCs are presented in Figure 10,

Table 1 | Kinetic parameters for the adsorption of NOR and CIP onto Fe-Cu-NCs

T/K	NOR			CIP		
C_0/(mmol/L)	0.313	0.470	0.626	0.313	0.470	0.626
Pseudo-first order						
$k_1 \times 10$/(min^{-1})	1.552	1.728	2.037	4.794	3.944	4.170
q_e(exp)/(mmol/g)	0.906	1.038	1.153	0.592	0.787	0.871
q_e(cal)/(mmol/g)	0.749	0.882	0.981	0.500	0.647	0.718
R^2	0.811	0.848	0.850	0.849	0.825	0.840
ARS	0.226	0.199	0.186	0.146	0.162	0.152
Pseudo-second order						
k_2/(g/(mmol·min))	0.273	0.263	0.278	1.223	0.765	0.748
q_e(cal)/(mmol/g)	0.806	0.953	1.056	0.532	0.692	0.766
R^2	0.911	0.936	0.938	0.924	0.912	0.920
ARS	0.158	0.132	0.122	0.105	0.117	0.108
Double-constant rate equation						
a	0.321	0.406	0.481	0.316	0.382	0.436
K_s	0.196	0.183	0.170	0.119	0.134	0.128
R^2	0.999	0.998	0.998	0.997	0.996	0.997
ARS	0.015	0.021	0.02	0.022	0.025	0.022
Elovich equation						
A	0.948	1.503	2.413	13.857	7.789	11.905
B	8.477	7.480	7.087	18.629	13.059	12.242
R^2	0.992	0.996	0.997	0.992	0.990	0.991
ARS	0.054	0.034	0.028	0.035	0.041	0.036
Intra-particle diffusion						
k_{t1}/(mmol/(g·$min^{0.5}$))	0.063	0.082	0.087	0.026	0.039	0.044
C_1/(mmol/g)	0.292	0.344	0.418	0.323	0.387	0.437
R	0.998	0.998	0.997	0.996	0.999	0.996
k_{t2}/(mmol/(g·$min^{0.5}$))	0.031	0.032	0.033	0.015	0.023	0.025
C_2/(mmol/g)	0.472	0.616	0.719	0.392	0.473	0.535
R	0.978	0.999	0.997	0.971	0.996	0.992

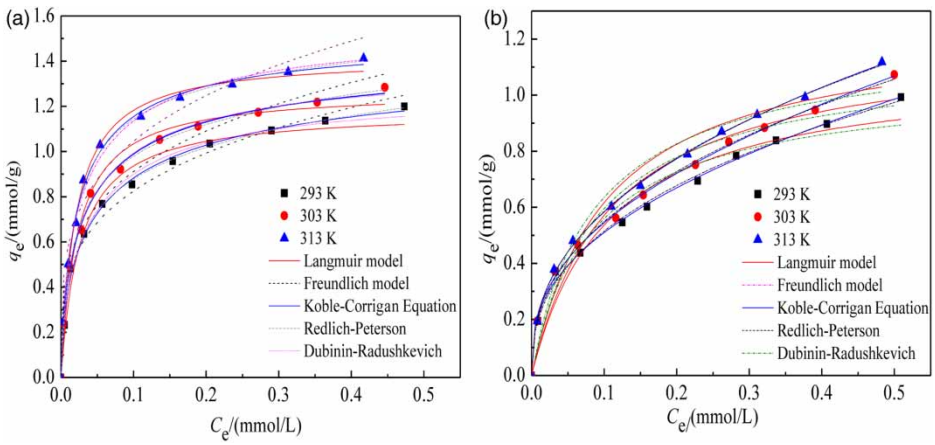

Figure 10 | Adsorption isotherms for the adsorption of NOR (a) and CIP (b) onto Fe-Cu-NCs.

Table 2 | Parameters of adsorption isotherm for NOR and CIP onto Fe-Cu-NCs

Isotherm models	NOR			CIP		
	293 K	303 K	313 K	293 K	303 K	313 K
Langmuir						
$q_{m,cal}$/(mmol/g)	1.182	1.271	1.421	1.103	1.202	1.246
$q_{m,exp}$/(mmol/g)	1.199	1.284	1.412	0.993	1.073	1.118
K_L/(L/mmol)	38.072	43.599	49.520	9.461	9.058	9.792
R^2	0.979	0.985	0.993	0.952	0.958	0.966
ARS	0.098	0.098	0.091	0.218	0.224	0.203
Freundlich						
K_F/((mmol/g)(L/mmol)1/n)	1.880	1.526	1.655	1.282	1.401	1.491
$1/n$	0.255	0.267	0.259	0.397	0.407	0.407
R^2	0.957	0.978	0.970	0.997	0.998	0.999
ARS	0.280	0.197	0.222	0.040	0.030	0.032
Koble-Corrigan						
A	8.779	14.050	29.457	0.876	1.038	1.409
B	5.862	9.447	19.254	−0.357	−0.297	−0.064
n	0.611	0.677	0.796	0.317	0.343	0.395
R^2	0.995	0.995	0.997	0.997	0.998	0.999
ARS	0.076	0.062	0.026	0.046	0.037	0.035
Redlich-Peterson						
A	91.917	97.958	95.222	1.343×10^5	1.312×10^5	502.615
B	66.885	67.478	61.280	1.048×10^5	0.936×10^5	337.867
g	0.849	0.875	0.923	0.604	0.593	0.600
R^2	0.998	0.997	0.997	0.996	0.998	0.999
ARS	0.051	0.041	0.042	0.040	0.030	0.027
Dubinin-Radushkevich						
q_m/(mmol/g)	1.242	1.345	1.515	1.008	1.093	1.152
E_a/(kJ/mol)	7.271	7.499	7.698	5.385	5.298	5.354
R^2	0.994	0.996	0.995	0.954	0.958	0.967
ARS	0.055	0.057	0.057	0.185	0.198	0.177

and the relevant model parameters are listed in Table 2. It can be seen that the adsorption capacity of NOR and CIP increased with increasing solution temperature. When the temperature was increased from 293 to 313 K, the adsorption capacity of NOR was increased from 1.199 to 1.412 mmol/g, and that of CIP was increased from 0.993 to 1.118 mmol/g. This was due to the acceleration of originally slow adsorption or the creation of some new active sites on the adsorbent surface (Meng *et al.* 2018). This finding indicated that the process of adsorbing NOR and CIP molecules is apparently endothermic in nature. In addition, the initial concentration of NOR or CIP was positively correlated with the adsorption concentration when the temperature was kept constant. As can be seen from Figure 10, the maximum adsorption capacity of NOR onto Fe-Cu-NCs is greater than that of CIP, which is consistent with the kinetic results.

To better describe the adsorption behavior, the experimental data were examined with Langmuir, Freundlich, Koble-Corrigan, Redlich-Peterson and Dubinin-Radushkevich models. These models can be described by the following

equations:

$$\text{Langmuir model: } q_e = \frac{q_m K_L C_e}{1 + K_L C_e} \quad (9)$$

$$\text{Freundlich model: } q_e = K_F C_e^{1/n_F} \quad (10)$$

$$\text{Redlich-Peterson model: } q_e = \frac{A_R C_e}{1 + B_R C_e^g} \quad (11)$$

$$\text{Koble-Corrigan model: } q_e = \frac{A C_e^{n_{KC}}}{1 + B C_e^{n_{KC}}} \quad (12)$$

$$\text{Dubinin-Radushkevich: } q_e = q_m \exp\left[(RT \ln(1 + 1/C_e))^2/(-2E^2)\right] \quad (13)$$

where C_e (mmol/L) is the equilibrium concentration of the solution and q_e (mmol/g) is the equilibrium adsorption capacity. q_m (mmol/g) is the theoretical maximum adsorption capacity and K_L (L/mmol) is the Langmuir constant related to rate of adsorption. K_F ((mmol/g) (L/mmol)$^{1/n}$) and n_F are the Freundlich constants that give a measure of adsorption capacity and adsorption intensity, respectively. E (kJ/mol) is the energy of adsorption of the Dubinin-Radushkevich model. A_R, B_R and g are the Redlich-Peterson parameters and n_{KC} is an indicator of the adsorption intensity of the Koble-Corrigan model.

From Table 2, based on the high correlation coefficient R^2 and low relative standard deviation ARS, the adsorption isotherm models fitted to the equilibrium data of NOR on Fe-Cu-NCs were in the following sequence: Redlich-Peterson > Koble-Corrigan > Dubinin-Radushkevich > Langmuir > Freundlich. Both the Redlich-Peterson model and the Koble-Corrigan model contain three parameters and combine the characteristics of the Langmuir and the Freundlich isotherms models. According to the data in Table 2, the constant g of the Redlich-Peterson model was close to 1, indicating that the NOR adsorption process was approaching the Langmuir model (Wan *et al.* 2018). The Koble-Corrigan model also fitted the experimental data better and the parameter n_{KC} of Koble-Corrigan model was between 0 and 1 (0.611–0.796), indicating that the adsorption of NOR onto Fe-Cu-NCs was more complex. It can be seen that the correlation coefficient of the Langmuir model (R^2: 0.979–0.993) was higher than that of the Freundlich model (R^2: 0.957–0.970) and the values of $q_{m,cal}$ obtained by the Langmuir model were closer to the values of $q_{m,exp}$. It was verified that the Langmuir model could better describe NOR adsorption onto Fe-Cu-NCs. The maximum q_m obtained from the Langmuir model were found to be 1.199 to 1.412 mmol/g as the temperature increased from 293 K to 313 K, which were higher than most of the adsorbents previously reported (Table 3).

Table 3 | Comparison of maximum adsorption capacities of NOR and CIP on different adsorbents

Materials	Adsorbates	q_m(mmol/g)	References
Polydopamine microspheres	NOR	0.961	Wan *et al.* (2018)
Layered chalcogenide	NOR	0.733	Li *et al.* (2018)
Magnetic copper-based metal organic frameworks	NOR	1.606	Wu *et al.* (2018)
Magnetic biochar	NOR	0.520	Liu *et al.* (2019)
Fe,Cu oxide nanocomposites	NOR	1.182	This work
Magnetic copper based metal-organic frameworks	CIP	1.463	Wu *et al.* (2018)
Layered chalcogenide	CIP	0.694	Li *et al.* (2018)
$CoFe_2O_4$/Activated carbon@Chitosan	CIP	0.513	Malakootian *et al.* (2018)
Montmorillonite	CIP	1.033	Wu *et al.* (2010)
Fe,Cu oxide nanocomposites	CIP	1.103	This work

The Dubinin-Radushkevich model can be applied to distinguish physical or chemical adsorption based on the adsorption free energy. Application of the Dubinin-Radushkevich model gave the adsorption free energies of 3.87, 4.11 and 4.32 kJ/mol at 293 K, 303 K and 313 K, respectively. The values were lower than 8.00 kJ/mol, indicating that NOR adsorption onto Fe-Cu-NCs was dominated by physisorption (Martins *et al.* 2015).

The adsorption isotherm models fitted the equilibrium data of CIP onto Fe-Cu-NCs in the following sequence: Koble-Corrigan > Redlich-Peterson > Freundlich > Dubinin-Radushkevich > Langmuir. The Koble-Corrigan model and the Redlich-Peterson model fitted the experimental date better. The constant g of the Redlich-Peterson model was far less than 1, indicating that the CIP adsorption process had the behavior of the Freundlich model. According to the values of R^2 and ARS, the Freundlich model was more suitable for describing the adsorption behavior of CIP onto Fe-Cu-NCs. The values of $1/n_F$ (0.397–0.407) were less than 0.5, indicating a favorable adsorption for CIP onto Fe-Cu-NCs. For the Dubinin-Radushkevich

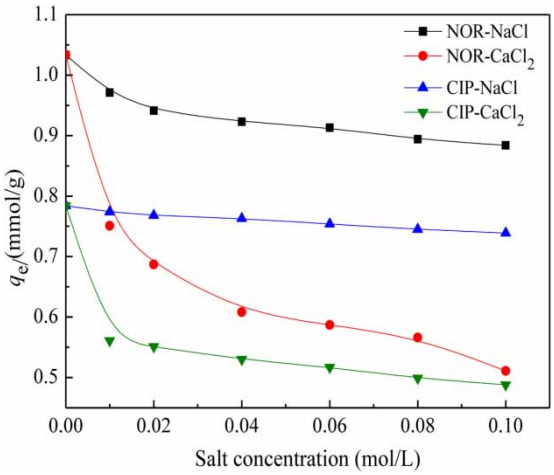

Figure 11 | Effects of ionic (Na^+ and Ca^{2+}) concentration on NOR and CIP adsorption onto Fe-Cu-NCs.

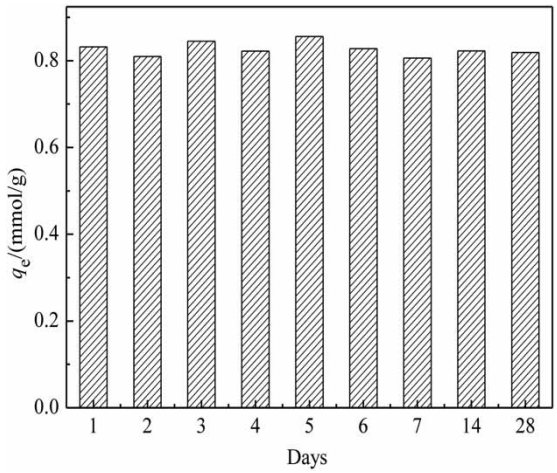

Figure 12 | CIP adsorption capacity of Fe-Cu-NCs stored for 1–28 days.

model, the values of E_a were 2.92, 3.15 and 3.23 kJ/mol at 293 K, 303 K and 313 K, respectively, indicating that the CIP adsorption onto Fe-Cu-NCs was also dominated by physisorption.

The effect of ionic strength

As shown in Figure 11, the adsorption of NOR and CIP onto Fe-Cu-NCs decreased with increasing ionic strength. The adsorption amounts of NOR and CIP onto Fe-Cu-NCs were reduced by 0.522 and 0.296 when the $CaCl_2$ concentration increased from 0 to 0.1 mol/L in aqueous solution, respectively. Conversely, with the increase of NaCl concentration from 0 to 0.1 mol/L, the adsorption amounts of NOR and CIP showed no obvious change, with reductions of 0.149 and 0.045, respectively. These results would be due to the fact that the adsorption capacity of antibiotics onto Fe-Cu-NCs was affected by the competitive adsorption of Na^+ and Ca^{2+} ions in solution. The increase of ionic concentration can reduce the active sites of the adsorbent, which confirmed the existence of electrostatic interactions between NOR or CIP and the Fe-Cu-NCs (Wan *et al.* 2018). Ca^{2+} had a stronger inhibitory effect on adsorption, not only because of its higher positive charge, but also because of its complexation effect with NOR or CIP. Furthermore, Ca^{2+} was easily combined with the oxygen atom of the carbonyl group and one of the two oxygen atoms of the carboxyl group on the NOR or CIP to form a stable six-membered ring, which may have restricted the positive contribution of hydrogen bonding to the adsorption process, thus leading to a reduction in NOR or CIP adsorption (Al-Mustafa 2002).

Stability of adsorption properties of Fe-Cu-NCs

As shown in Figure 12, the stability of Fe-Cu-NCs as adsorbents was studied. It was found that the change of adsorption capacity of CIP onto Fe-Cu-NCs was slight, indicating that the Fe-Cu-NCs were stable over an extended time period. The organic matter capping on the adsorbent surface and the added oxalic acid played an important role in the stability of the Fe-Cu-NCs. (Zhang *et al.* 2018).

Adsorption thermodynamic study

The Gibbs free energy change (ΔG), enthalpy change (ΔH) and entropy change (ΔS) were calculated using the following equations:

$$\Delta G = -RT \ln K_c \tag{14}$$

$$\Delta G = \Delta H - T\Delta S \tag{15}$$

where K_c is the thermodynamic equilibrium constant. T (K) is temperature in Kelvin, and R is the universal gas constant (8.314 J/(mol K)).

For the adsorption of NOR onto Fe-Cu-NCs, the positive values of ΔH and ΔS were 2.72 kJ/mol and 22.5 J/(mol K), respectively. The value of ΔH was less than 40 kJ/mol, which indicated that the adsorption process was endothermic in nature and controlled by physical adsorption (Zhou *et al.* 2017). The ΔG values were −3.87, −4.11, −4.32 kJ/mol at 293, 303 and 313 K, respectively, indicating

that the NOR adsorption process was feasible and spontaneous. The negative value of ΔG decreased with increasing solution temperature, indicating that the adsorption of NOR onto Fe-Cu-NCs became more favorable at higher temperatures (Ponnusamy *et al.* 2010).

For the adsorption of CIP onto Fe-Cu-NCs, the values of ΔH and ΔS were 1.6 kJ/mol and 15.5 J/(mol K), respectively. The ΔG values were −2.92, −3.15, −3.23 kJ/mol at 293, 303 and 313 K, respectively. The process of adsorption was also an endothermic and spontaneous process.

CONCLUSIONS

In this study, Fe-Cu-NCs were successfully synthesized from loquat leaf extracts and used in the adsorption process of NOR and CIP from aqueous solution. SEM, TEM, XPS, XRD and FTIR verified the spherical structure and possible surface composition of biomolecules and surface functional groups of the Fe-Cu-NCs, which provided a basis for the excellent adsorption capacity. The results of kinetic study showed the adsorption process fitted the double-constant rate equation and the Elovich model well, and both film diffusion and intra-particle diffusion control the adsorption process. The equilibrium data suggested that the NOR and CIP adsorption onto Fe-Cu-NCs was favorable and dominated by physisorption. In addition, the thermodynamic parameters (ΔG, ΔH, and ΔS) indicated that the adsorption of NOR and CIP onto Fe-Cu-NCs was spontaneous and endothermic. The adsorption performance of the Fe-Cu-NCs for NOR and CIP may be attributed to electrostatic interaction, hydrogen bonding, hydrophobic interaction, n-π electron donor–acceptor (EDA) interactions and surface complexation. In this study, Fe-Cu-NCs showed good stability and high adsorption, and their synthesis process is green and harmless. Thus, Fe-Cu-NCs are considered to be a potential and excellent adsorbents for the removal of antibiotic wastewater. They provide a new insight into applications for the remediation of other pollutants.

ACKNOWLEDGEMENTS

This work was supported by the Henan Science and Technology Department in China (No. 162300410016) and program of biomass resources processing and efficient utilization of outstanding foreign scientists' workroom (GZS2018004).

REFERENCES

Al-Mustafa, J. 2002 Magnesium, calcium and barium perchlorate complexes of ciprofloxacin and norfloxacin. *Acta Chim. Slov.* **49**, 457–466.

Al-Musawi, T. J., Brouers, F. & Zarrabi, M. 2017 Kinetic modeling of antibiotic adsorption onto different nanomaterials using the Brouers–Sotolongo fractal equation. *Environ. Sci. Pollut. Res.* **24** (4), 4048–4057.

Anthony, A. A., Adekunle, C. F. & Thor, A. S. 2018 Residual antibiotics, antibiotic resistant superbugs and antibiotic resistance genes in surface water catchments: public health impact. *Phys. Chem. Earth* Parts A/B/C **105**, 177–183.

Awwad, A. M., Salem, N. M. & Abdeen, A. O. 2013 Green synthesis of silver nanoparticles using carob leaf extract and its antibacterial activity. *Int. J. Ind. Chem.* **4** (1), 1–6.

Fang, Z., Qiu, X., Chen, J. & Qiu, X. 2011 Debromination of polybrominated diphenyl ethers by Ni/Fe bimetallic nanoparticles: influencing factors, kinetics, and mechanism. *J. Hazard. Mater.* **185** (2–3), 958–969.

Grosvenor, A. P., Kobe, B. A., Biesinger, M. C. & McIntyre, N. S. 2004 Investigation of multiplet splitting of Fe 2p XPS spectra and bonding in iron compounds. *Surf. Interface Anal.* **36** (12), 1564–1574.

Gutiérrez, M. S., Duel, P., Hierro, F., Morey, J. & Piña, M. N. 2018 A very highly efficient magnetic nanomaterial for the removal of PAHs from aqueous media. *Small* **14** (8), 1702573.

He, Y., Jiang, D. B., Chen, J., Jiang, D. Y. & Zhang, Y. X. 2018 Synthesis of MnO_2 nanosheets on montmorillonite for oxidative degradation and adsorption of methylene blue. *J. Colloid Interface Sci.* **510**, 207–220.

Homem, V. & Santos, L. 2011 Degradation and removal methods of antibiotics from aqueous matrices – a review. *J. Environ. Manage.* **92** (10), 2304–2347.

Jha, D., Mubarak, N. M., Haider, M. B., Kumar, R., Balathanigaimani, M. S. & Sahu, J. N. 2019 Adsorptive removal of dibenzothiophene from diesel fuel using microwave synthesized carbon nanomaterials. *Fuel* **244**, 132–139.

Khandare, D. & Mukherjee, S. 2019 A review of metal oxide nanomaterials for fluoride decontamination from water environment. *Mater. Today: Proc.* **18**, 1146–1155.

Kong, Q., Wang, Y., Shu, L. & Miao, M. 2016 Isotherm, kinetic, and thermodynamic equations for cefalexin removal from liquids using activated carbon synthesized from loofah sponge. *Desalin. Water Treat.* **57** (17), 7933–7942.

Li, J., Xu, L., Fu, M. & Lan, H. 2018 Can adsorbent of layered chalcogenide be regenerated? A case study of norfloxacin adsorbed by layered chalcogenide in water. *Colloids Surf. A Physicochem. Eng. Aspects* **537**, 287–293.

Liu, W., Zhang, J., Zhang, C. & Ren, L. 2011 Sorption of norfloxacin by lotus stalk-based activated carbon and iron-doped activated alumina: mechanisms, isotherms and kinetics. *Chem. Eng. J.* **171** (2), 431–438.

Liu, X., Wan, Y., Liu, P., Zhao, L. & Zou, W. 2019 Optimization of sulfamethazine sodium adsorption onto activated carbon-based *Salix psammophila*: investigation of adsorption behavior and mechanism. *J. Dispersion. Sci. Technol.* **40** (4), 507–518.

Luo, F., Yang, D., Chen, Z., Megharaj, M. & Naidu, R. 2015 The mechanism for degrading Orange II based on adsorption and reduction by ion-based nanoparticles synthesized by grape leaf extract. *J. Hazard. Mater.* **296**, 37–45.

Makarov, V. V., Makarova, S. S., Love, A. J., Sinitsyna, O. V., Dudnik, A. O., Yaminsky, I. V., Taliansky, M. E. & Kalinina, N. O. 2014 Biosynthesis of stable iron oxide nanoparticles in aqueous extracts of *Hordeum vulgare* and *Rumex acetosa* plants. *Langmuir* **30** (20), 5982–5988.

Malakootian, M., Nasiri, A. & Mahdizadeh, H. 2018 Preparation of $CoFe_2O_4$/activated carbon@chitosan as a new magnetic nanobiocomposite for adsorption of ciprofloxacin in aqueous solutions. *Water Sci. Technol.* **78** (10), 2158–2170.

Martins, A. C., Pezoti, O., Cazetta, A. L., Bedin, K. C., Yamazaki, D. A. S., Bandoch, G. F. G., Asefa, T., Visentainer, J. V. & Almeida, V. C. 2015 Removal of tetracycline by NaOH-activated carbon produced from macadamia nut shells: kinetic and equilibrium studies. *Chem. Eng. J.* **260**, 291–299.

Meng, C., Zhikun, W., Qiang, L., Chunling, L., Shuangqing, S. & Songqing, H. 2018 Preparation of amino-functionalized Fe_3O_4@$mSiO_2$ core-shell magnetic nanoparticles and their application for aqueous Fe^{3+} removal. *J. Hazard. Mater.* **341**, 198–206.

Mohan Kumar, K., Mandal, B. K., Siva Kumar, K., Sreedhara Reddy, P. & Sreedhar, B. 2013 Biobased green method to synthesise palladium and iron nanoparticles using *Terminalia chebula* aqueous extract. *Spectrochim. Acta A* **102**, 128–133.

Nalbandian, M. J., Zhang, M., Sanchez, J., Choa, Y. H., Nam, J., Cwiertny, D. M. & Myung, N. V. 2016 Synthesis and optimization of Fe_2O_3 nanofibers for chromate adsorption from contaminated water sources. *Chemosphere* **144**, 975–981.

Ponnusamy, S. K., Subramaniam, R., Senthamarai, C., Niranjanaa, M., Vijayalakshmi, P. & Sivanesan, S. 2010 Adsorption of dye from aqueous solution by cashew nut shell: studies on equilibrium isotherm, kinetics and thermodynamics of interactions. *Desalination* **261**, 52–60.

Sai Saraswathi, V., Tatsugi, J., Shin, P. & Santhakumar, K. 2017 Facile biosynthesis, characterization, and solar assisted photocatalytic effect of ZnO nanoparticles mediated by leaves of L. speciosa. *J. Photochem. Photobiol. B: Biol.* **167**, 89–98.

Sepehr, M. N., Amrane, A., Karimaian, K. A., Zarrabi, M. & Ghaffari, H. R. 2014 Potential of waste pumice and surface modified pumice for hexavalent chromium removal: characterization, equilibrium, thermodynamic and kinetic study. *J. Taiwan Inst. Chem. Eng.* **45** (2), 635–647.

Singh, D. K., Verma, D. K., Singh, Y. & Hasan, S. H. 2017 Preparation of CuO nanoparticles using *Tamarindus indica* pulp extract for removal of As(III): optimization of adsorption process by ANN-GA. *J. Environ. Chem. Eng.* **5** (1), 1302–1318.

Sun, X., Han, F., Wang, H., Song, F., Cui, X., Lou, Y. & Zhuge, Y. 2019 Characterization of three Pb-resistant fungi and their potential Pb^{2+} ions adsorption capacities. *Water Sci. Technol.* **78** (12), 2616–2625.

Wan, Y., Liu, X., Liu, P., Zhao, L. & Zou, W. 2018 Optimization adsorption of norfloxacin onto polydopamine microspheres from aqueous solution: kinetic, equilibrium and adsorption mechanism studies. *Sci. Total Environ.* **639**, 428–437.

Wang, L. & Yan, G. 2011 Adsorptive removal of direct yellow 161dye from aqueous solution using bamboo charcoals activated with different chemicals. *Desalination* **274** (1–3), 81–90.

Wang, T., Jin, X., Chen, Z., Megharaj, M. & Naidu, R. 2014 Green synthesis of Fe nanoparticles using eucalyptus leaf extracts for treatment of eutrophic wastewater. *Sci. Total Environ.* **466–467**, 210–213.

Weng, X., Guo, M., Luo, F. & Chen, Z. 2017 One-step green synthesis of bimetallic Fe/Ni nanoparticles by eucalyptus leaf extract: Biomolecules identification, characterization and catalytic activity. *Chem. Eng. J.* **308**, 904–911.

Wu, Q., Li, Z., Hong, H., Yin, K. & Tie, L. 2010 Adsorption and intercalation of ciprofloxacin on montmorillonite. *Appl. Clay Sci.* **50** (2), 204–211.

Wu, G., Jiping, M., Shuang, L., Jing, G., Bo, J., Liyan, W., Jinhua, L., Xiaoyan, W. & Lingxin, C. 2018 Magnetic copper-based metal organic framework as an effective and recyclable adsorbent for removal of two fluoroquinolone antibiotics from aqueous solutions. *J. Colloid Interf. Sci.* **528**, 360–371.

Yadav, M., Mun, S., Hyun, J. & Kim, J. 2015 Synthesis and characterization of iron oxide/cellulose nanocomposite film. *Int. J. Biol. Macromol.* **74**, 142–149.

Yang, W., Lu, Y., Zheng, F., Xue, X., Li, N. & Liu, D. 2012 Adsorption behavior and mechanisms of norfloxacin onto porous resins and carbon nanotube. *Chem. Eng. J.* **179**, 112–118.

Yuan, L., Yan, M., Huang, Z., He, K., Zeng, G., Chen, A., Hu, L., Li, H., Peng, M., Huang, T. & Chen, G. 2019 Influences of pH and metal ions on the interactions of oxytetracycline onto nano-hydroxyapatite and their co-adsorption behavior in aqueous solution. *J. Colloid Interf. Sci.* **541**, 101–113.

Zhang, Y., Wu, B., Xu, H., Liu, H., Wang, M., He, Y. & Pan, B. 2016 Nanomaterials-enabled water and wastewater treatment. *NanoImpact* **3–4**, 22–39.

Zhang, P., Hou, D., O'Connor, D., Li, X., Pehkonen, S., Varma, R. S. & Wang, X. 2018 Green and size-specific synthesis of stable Fe–Cu oxides as earth-abundant adsorbents for Malachite Green removal. *ACS Sustain. Chem. Eng.* **6** (7), 9229–9236.

Zheng, H., Wang, Z., Zhao, J., Herbert, S. & Xing, B. 2013 Sorption of antibiotic sulfamethoxazole varies with biochars produced at different temperatures. *Environ. Pollut.* **181**, 60–67.

Zhou, J., Lü, Q. & Luo, J. 2017 Efficient removal of organic dyes from aqueous solution by rapid adsorption onto polypyrrole–based composites. *J. Cleaner Prod.* **167**, 739–748.

First received 24 December 2019; accepted in revised form 20 March 2020. Available online 3 April 2020